

REGULAR PAPER



Janus shaped plasmonic-magnetic silver-magnetite nanostructures for multimodal applications

To cite this article: Pinki Singh *et al* 2019 *Jpn. J. Appl. Phys.* **58** 105001

View the [article online](#) for updates and enhancements.



Janus shaped plasmonic-magnetic silver-magnetite nanostructures for multimodal applications

Pinki Singh^{1*} , Purnima Bharti¹, Asnit Gangwar², Nand Kishore Prasad², and Chandan Upadhyay^{1*} 

¹School of Materials Science and Technology, Indian Institute of Technology (Banaras Hindu University), Varanasi, 221005, India

²Department of Metallurgical Engineering, Indian Institute of Technology (Banaras Hindu University), Varanasi, 221005, India

*E-mail: psingh.rs.mst13@itbhu.ac.in; cupadhyay.mst@itbhu.ac.in

Received July 2, 2019; revised July 25, 2019; accepted August 18, 2019; published online September 11, 2019

The multifunctional biocompatible Janus shaped plasmonic-magnetic silver-magnetite nanoparticles have been developed via a single phase microemulsion technique and investigated for different physical properties. The noble metal integration with magnetite nanoparticles introduces superior optical properties into the nanostructures. The dynamic light scattering technique has been used to measure the hydrodynamic size, monodispersity and zeta potential to check their suitability as multimodal agents. The synthesized silver-magnetite nanoparticles are monodispersed and possess colloidal stability. The UV-visible spectra for Janus silver-magnetite nanoparticles shows a surface plasmon resonance peak at 372 and 474 nm which lies in the visible region of electromagnetic spectrum. The photoluminescence spectrum confirms the obtained nanoparticles to be optically active. The measurements of response for bare magnetite as well as silver-magnetite nanoparticles in an alternating magnetic field reveal their suitability in hyperthermia applications. These synthesized integrated magnetite-silver nanostructures show its potential as an excellent candidate for multimodal applications. © 2019 The Japan Society of Applied Physics

1. Introduction

The study of iron oxide nanoparticles with different size, shape and functionalization is being carried out worldwide due to their superior magnetic properties,¹ ease in synthesis,² low cost preparation,³ specific biodistribution⁴ and high magnetic permeability.⁵ They have also been approved by the food and drug administration, USA, which implies their suitability in biomedical applications.⁶ Among various iron oxide nanoparticles available, magnetite shows the highest magnetic response at room temperature and behaves as either ferrimagnetic or superparamagnetic below a critical particle size.⁷ The iron oxide nanoparticles can be effectively stimulated by application of alternating magnetic fields to produce heat since they have no barrier to penetration depth.⁸

In recent years, much effort has been made to improve the optical behavior of the magnetic materials so that they can be employed as multimodal agents.^{9,10} The integration of magnetite nanostructures with fluorescent dyes, rare-earth complexes and polymers fulfill this requirement but has a number of drawbacks e.g. toxicity, sensitivity and photo-bleaching.¹¹ The attachment of noble metals with magnetite nanoparticles such as silver or gold is employed to overcome these limitations. The selection of noble materials is done due to their superior optical properties which are highly tunable. This tunability increases manifold on the modification in their integrated structure. The core-shell structure is found to have an excellent optical tunability of absorption wavelength along the entire visible and near UV range for a core-shell ratio of 12:1 and 16:1 for gold and silver shell coated magnetite nanoparticles, respectively, for smaller particle size.^{12,13} Although, they exhibit superior optical properties but decrease in their magnetization is observed which is due to the shielding of the magnetic core with non-magnetic shell. To overcome this drawback, noble metal integrated magnetic nanoparticles with Janus shape can be taken into account which will possibly have a minor impact on the magnetization values of magnetite nanoparticles.

Till now, there is limited study on the synthesis methods and physical properties of silver-magnetite Janus structured systems. In this paper, we have investigated the different physical parameters such as their phase purity, particle size, hydrodynamic size when dispersed in water, zeta potential, absorption wavelength, band gap and hyperthermic response of the iron oxide based nanoparticles that also play a crucial role in implementation of these particles for various applications. The sample is synthesized in a single phase emulsion solution which requires no high temperature treatment and is cost-effective. The synthesized nanoparticles are found to be highly stable and display good hyperthermic response.

2. Experimental

The synthesis of Janus shaped silver-magnetite nanoparticles is carried out in two steps as reported in a prior article for core-shell structure with minor modifications:¹⁴ (i) formation of magnetite in single phase emulsion solution, (ii) silver integration of obtained magnetite nanoparticles via the coprecipitation method. The salts ferrous and ferric ammonium sulfates were weighed in the ratio 1:2 and dissolved in aqueous sulphuric acid (solution I). Another solution containing a pre-determined molar concentration of sodium hydroxide and cetyltrimethylammonium bromide (CTAB) introduced as surfactant was prepared (solution II). Solution II was then stirred and heated in a constant temperature bath ($T \sim 70$ °C) for few minutes into which solution I is added drop wise. The resultant solution is stirred and heated for another 30 min. The magnetite nanoparticles are obtained as black suspended mass which is washed and separated using ultrasonication and centrifugation. The nanoparticles are then dried at reaction temperature in vacuum for another 24 h.

The magnetite nanoparticles are weighed and dispersed in distilled water. The amount of silver nitrate required to coat the magnetite with desirable shell thickness was calculated, weighed and mixed in distilled water. NaOH and glucose were added to the magnetite solution. In this solution, the silver nitrate solution is mixed drop by drop. The mixed solution is allowed to heat and stir for another 12 h. The silver-magnetite nanoparticles are washed and separated from

the solution. The nanoparticles obtained are dried at reaction temperature i.e. 50 °C in vacuum. The glucose is employed to restrict the growth of any individual silver nanoparticles.

The uncoated and silver-magnetic samples were characterized for their structural investigation using an X-ray diffractometer (Rigaku, Japan) with $\text{CuK}\alpha$ radiation for a scan range of 20 to 80 degrees. The particle size and shape of the synthesized particles were obtained using transmission electron microscopy (FEI TECNAI G2 20 TWIN Type) operated at 200 kV. The monodispersity, hydrodynamic particle size and zeta potential of the nanoparticles dispersed in ultrapure water were analyzed with the help of a dynamic light scattering particle size analyzer (Horiba Scientific nanopartica SZ-100 series). The UV-visible (UV-vis) spectrophotometer (Hitachi, U-3010) was used to estimate the absorption wavelength. The band gap of the uncoated and coated magnetite nanoparticles is determined using the tauc plot from the UV-vis data. The luminescence spectra were collected from Hitachi F-4600 fluorescence spectrometer using a xenon lamp as the excitation source. The hyperthermic measurements were performed at a setup consisting of an RF coil and a temperature probe to check the suitability of silver coated magnetite nanoparticles as hyperthermic agents. The sample was dispersed in oleic acid with concentration $0.01 \text{ mg } \mu\text{l}^{-1}$ and $0.02 \text{ mg } \mu\text{l}^{-1}$ for magnetite and Janus shaped silver-magnetite nanoparticles, respectively, and studied for a nominal frequency of 110 kHz and magnetic field amplitude of 25 mT.

3. Result and discussion

The single phase microemulsion method employed to synthesize the stand alone nanoparticles and biphasic nanoparticles with varying morphologies. The area of interest is to investigate the effect of several parameters such as surfactant to dispersed phase ratio, synthesis temperature, presence of co-surfactants, pH etc. In one phase region, obtained by a cut through ternary phase diagram for microemulsions, the radius of micelles formed inside the solution for nucleus growth depends linearly upon the water-to-surfactant molar ratio. The size of obtained nanoparticle is heavily dependent upon this micelle size. As the concentration of surfactant is increased, the shape of droplets or the micelles begins to vary from smaller spheres to spheres with larger radii, aggregated spheres, cylinders, inter-connected cylinders and bicontinuous networks. The size of droplets increases with the temperature as the earlier studies have shown that with rise in temperature, the droplets become more attractive. In the one-phase region, the spheres and cylinders are found to coexist as after a critical geometric limit of radius; $R_C = 0.67R_S$, all the spheres transform into cylindrical shapes.¹⁵⁾ Further increase in the temperature approaching closer to upper phase boundaries, the cylindrical droplets begin to interconnect that leads to the formation of bicontinuous networks. The appropriate region for the formation of small-sized bare magnetite and silver-magnetite nanospheres is identified in the ternary phase diagram which led to the choice of single-phase solution for the current study.

The X-ray diffraction (XRD) patterns for synthesized magnetite and silver-magnetite nanoparticles are shown in Fig. 1. The analysis of XRD patterns in Fig. 1(a) indicates the formation of cubic spinel magnetite nanoparticles in pure

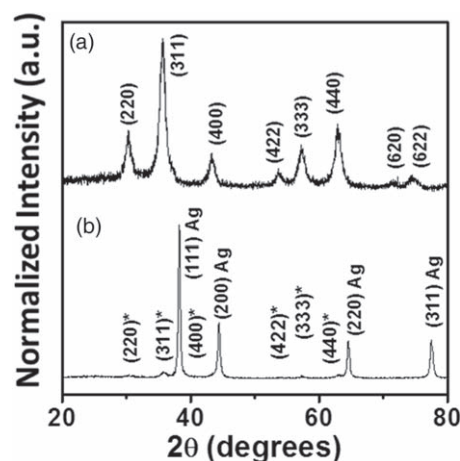


Fig. 1. XRD spectra for synthesized nanoparticles (a) pure phase Fe_3O_4 nanoparticles; (b) silver-magnetite Janus nanoparticles (* represents the peaks corresponding to Fe_3O_4 phase in core-shell structure).

phase (space group $\text{Fd}\bar{3}\text{m}$, 227). The XRD pattern for silver-magnetite nanoparticles [Fig. 1(b)] shows the presence of silver with space group $\text{Fm}\bar{3}\text{m}$, 225 along with the characteristic peaks of magnetite. The larger FWHM values in the XRD spectra indicates the formation of nanoparticles for both the samples. The crystallite size of pure phase magnetite nanoparticles is found to be 8 nm, calculated using Scherrer formula:¹⁶⁾ $d_{\text{cry}} = \frac{0.9\lambda}{\beta \cos \theta}$; where λ , β and θ are wavelength of incident $\text{CuK}\alpha$ radiation, FWHM and Bragg's angle. The X-ray diffractograms for silver-magnetite nanoparticles shows reflections corresponding to magnetite as well, with relatively very low intensity possibly due to the higher concentration of silver. The lower intense peaks of magnetite in silver coated magnetite nanoparticles hint towards coating of silver on the magnetite core.

Figure 2 represents the transmission electron microscopy (TEM) images and particle size distribution of the synthesized particles. The size distribution and average particle size of the uncoated and silver-magnetite nanoparticles were obtained by measuring size of nearly 200 particles using TEM micrographs. The histograms were fitted using log-normal distribution function to calculate the average particle size and its standard deviation. The mean particle size was found to be 8 nm for pure phase magnetite nanoparticles. In the case of silver- Fe_3O_4 Janus nanoparticles, the average particle size was found to be 10 nm. The presence of contrast in TEM images for silver-magnetite Janus nanoparticles is observed due to varying electron penetration efficiency for different elements. The lognormal fit of histograms for magnetite and silver-magnetite nanoparticles gives a standard deviation of 0.18 and 0.14, respectively that emphasizes on narrow size distribution of synthesized nanoparticles. The monodispersity of magnetite and silver-magnetite nanoparticles is also evident from the measurements of auto-correlation function versus delay time plot performed using dynamic light scattering (DLS). A single curve is observed in the graph which confirms the presence of monodispersed particles in the solution for magnetite as well as silver-magnetite Janus samples (inset of Fig. 3). The hydrodynamic size of the magnetite and silver-magnetite nanoparticles is found to be 71 and 131 nm which is higher than the particle sizes obtained through TEM images (Fig. 3). The particle size

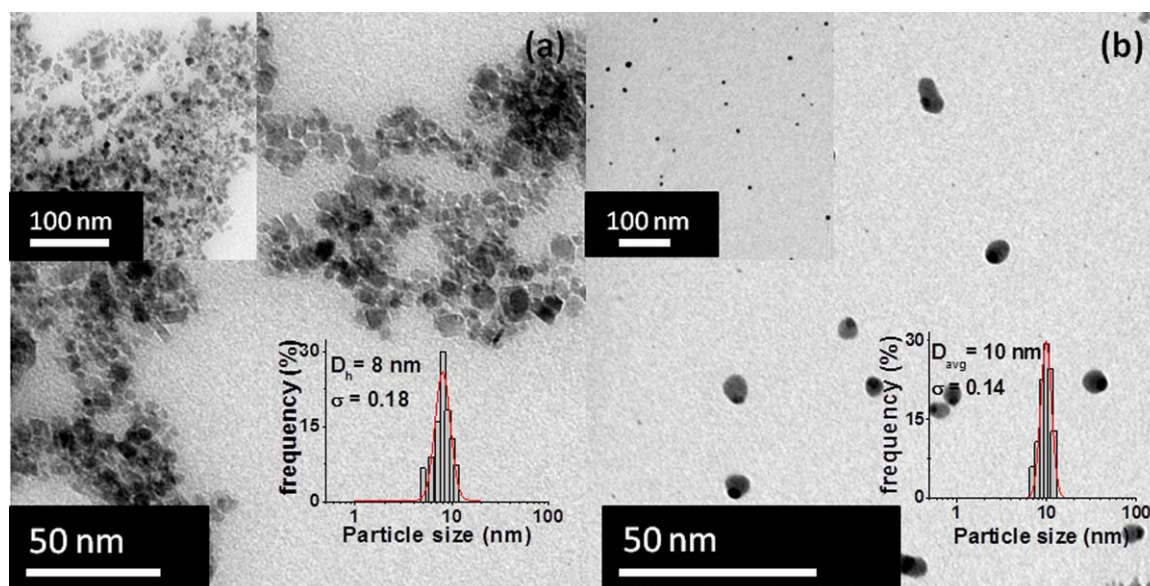


Fig. 2. (Color online) Transmission electron micrographs of (a) bare magnetite nanoparticles; (b) Janus silver-magnetite nanoparticles. The inset in figures represents particle size distribution and their lognormal fit with average particle size (D_{avg}) and standard deviation (σ). (Note: the size distribution histogram has been obtained using multiple TEM images.)

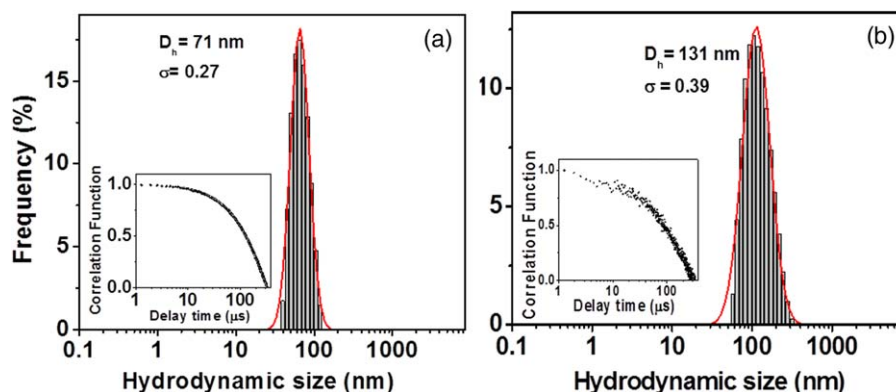


Fig. 3. (Color online) The particle size distribution chart obtained using the dynamic light scattering method to calculate hydrodynamic size (D_h) and standard deviation (σ) for (a) bare magnetite nanoparticles; (b) silver-magnetite nanoparticles. The insets in figure show variations of correlation function with delay time.

measured in TEM is for frozen samples in solid state whereas the size through DLS indicates the dynamic size of particles moving freely in the solvent.¹⁷⁾ This overall hydrodynamic size includes the interaction of nanoparticle interface with the solvent and the presence of any surfactant molecule on the surface.

The synthesized magnetite and silver-magnetite nanoparticles were found to be highly stable. The stability of colloidal nanoparticles dispersed in water has been concluded from zeta potential measurement of the nanoparticles. It is a measure of electric potential between charged entities at the surface of a nanoparticle and the dispersed medium. The zeta potential values lying in the range between 0 to ± 5 mV and ± 10 to ± 30 mV indicates rapid coagulation and nascent instability of samples, respectively.¹⁸⁾ The values in range ± 30 to ± 40 mV show moderate stability whereas ± 40 to ± 60 mV represents good stability of nanomaterials. Above ± 60 mV, the particles are considered to have excellent stability.¹⁹⁾ The zeta potential values obtained for magnetite and silver-magnetite nanoparticles are obtained to be -67.39 mV and -74.6 mV, respectively suggesting the

strongly electron rich nature of the nanoparticles. It can be inferred from the experimental values that synthesized samples, magnetite and silver-magnetite nanoparticles, are very highly stable. The integration of magnetite nanoparticles with silver increases the zeta potential resulting in enhancement of electrostatic repulsion among nanoparticles that further enhances its stability.^{20,21)}

The optical characteristics of the magnetite and silver-magnetite Janus structured samples have been studied in order to analyze their absorption wavelength and band gap. The noble metal nanoparticles such as gold and silver are known to show a surface plasmon resonance (SPR) peak/band in the visible region of electromagnetic spectrum (i.e., ~ 520 nm and ~ 420 nm, respectively).²²⁾ The SPR peak is observed due to resonance in the frequency of incident photon and collective oscillation of conduction electrons at the nanoparticle surface. The maximum absorption wavelength for a nanoparticle system is highly dependent upon its shape, size, dielectric properties, local environment and interparticle spacing.²³⁾ Figure 4 shows the measured UV-vis spectra for silver-magnetite nanoparticles. A SPR band at

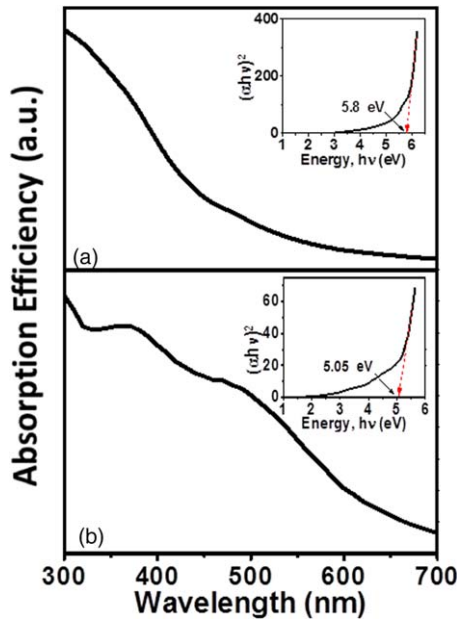


Fig. 4. (Color online) UV-vis spectra for synthesized nanoparticles (a) pure phase Fe_3O_4 nanoparticles; (b) Ag integrated Fe_3O_4 Janus nanoparticles. The inset in the figures show Tauc plots for the system to obtain their energy band gap.

372 nm and 474 nm corresponding to the silver-magnetite Janus nanoparticle appears in the spectrum. There is a noticeable shift and change in the nature of curve for the resonance peak position as compared to those for individual silver nanoparticles due to difference in morphology and local environment. The experimental band position is in agreement with those calculated theoretically using MATLAB simulation¹²⁾ while shape is not identical. The band gap of materials can also be evaluated using UV-vis absorption spectroscopy by employing the use of Tauc equation:²⁴⁾ $(\alpha h\nu)^2 = h\nu - E_g \phi$, where α and $h\nu$ represents the absorption co-efficient of nanoparticles and incident photon energy, respectively. The band gap of material is determined by extrapolating $(\alpha h\nu)^2$ to the incident photon energy axis which is found to be 5.7 eV and 4.9 eV for magnetite and silver- magnetite nanoparticles, respectively. The values of energy gap for magnetite nanomaterials have been reported to lie in the range 4–6 eV.²⁵⁾ The luminescence emission spectrum has also been recorded in a wavelength range of 420 nm to 700 nm upon illumination by an excitation wavelength of 390 nm. Two major emission peaks at 440 nm and 574 nm are observed for bare magnetite nanoparticles along with some less significant peaks. The silver integration with magnetite nanoparticle makes the two peaks more prominent and shift towards lower energy. The two maxima for silver-magnetite nanostructure appear at 450 nm and 587 nm with relatively larger intensities indicating an increase in the number of electrons participating in electron transfer from various energy levels due to match in energies between charge transfer band (CTB) of silver and Fe-O states.¹³⁾ The silver-magnetite nanoparticles have blue-emission in visible region of electromagnetic spectrum. The particles with blue-emission such as carbon-dots and nanoparticles have been studied to be useful in the detection of abnormal live cells due to their easy detection and identification.^{26,27)}

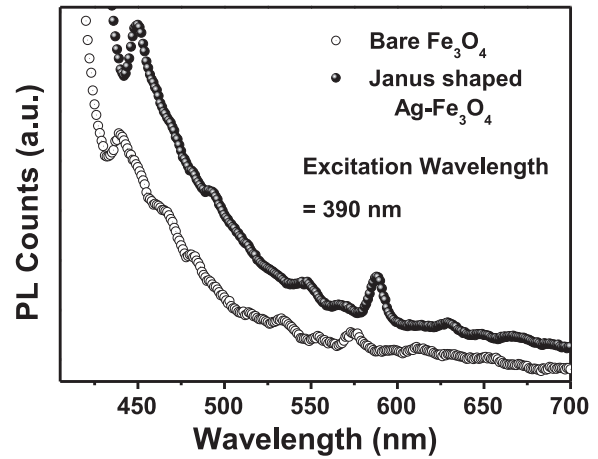


Fig. 5. Photoluminescence spectra for bare magnetite and silver-magnetite nanoparticles.

The magnetite and silver-iron oxide nanoparticles have been investigated for their application as hyperthermic agents. For nanoparticles of size smaller than 100 nm, heat can be generated with the help of two processes: relaxation via Néel and Brownian mechanism and hysteresis losses. In case of particles with diameter range in between 20–80 nm, which are multi-domain, the hysteresis loss dominates over any other phenomenon for heat generation. Particles with size less than 20 nm majorly consist of single magnetic domain which excludes the possibility for any kind of hysteresis loss. Thus, when the samples are exposed to alternating magnetic fields, the heat generation is mediated through Néel and Brownian relaxations.²⁸⁾ In humans, the normal body temperature ranges between 36.5 °C–37.5 °C. The human body tissues cannot bear temperature greater than 40 °C. This property of human cells/tissues is generally exploited to kill the abnormal tissues or tumors inside a patient. The hyperthermic response for Fe_3O_4 and silver- Fe_3O_4 nanoparticles have been recorded at a magnetic field of 25 mT and nominal frequency of 110 ± 1.0 kHz. For bare magnetite nanoparticles, with concentration $0.01 \text{ mg } \mu\text{l}^{-1}$, the temperature elevates from 31 °C to 46 °C in a span of merely 400 s (less than 10 min). In the case of silver-magnetite Janus nanoparticles, the temperature reaches 42 °C from 31 °C in a similar time span for a concentration of $0.02 \text{ mg } \mu\text{l}^{-1}$ dispersed in oleic acid. Figure 6 shows response of magnetite and silver-magnetite nanoparticles in the presence of alternating magnetic field. The hyperthermic response of materials is quantified by specific absorption rate (SAR), given by the equation, $\text{SAR} = \frac{C}{m} \left(\frac{dT}{dt} \right) \Big|_{t=0}$ that measures the efficiency of conversion from electromagnetic energy into heat. Here, C and m represents the heat capacity of dispersion medium and mass of suspended magnetic particles, respectively.²⁹⁾ The value $\left(\frac{dT}{dt} \right) \Big|_{t=0}$ denotes the initial rate of change in temperature with respect to time. The value of SAR is found to be equal to 7.58 W g^{-1} for bare magnetite and 1.28 W g^{-1} for silver-magnetite nanoparticles, when samples are placed in a vial of diameter 10 mm.

Based on the measurements and analysis carried out in the article, it is evident that integration with silver enhances the optical activity of nanoparticles in efficient manner. The

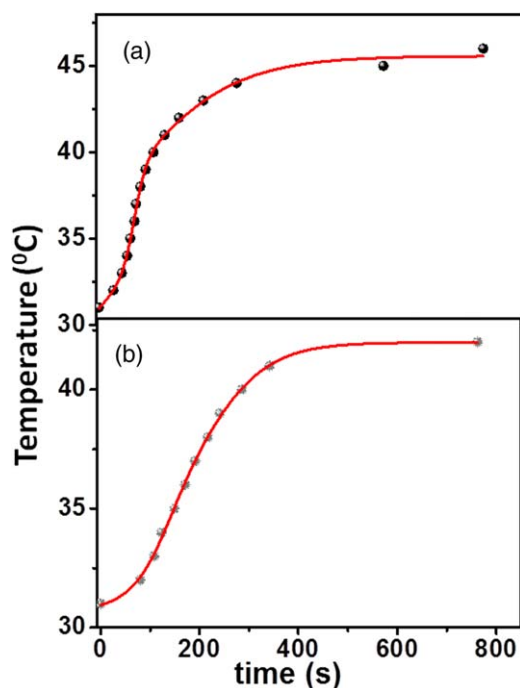


Fig. 6. (Color online) Temperature raise with elapsed time on application of alternating magnetic field 25 mT with frequency 110 kHz for (a) magnetite nanoparticles; (b) silver-magnetite Janus nanoparticles.

silver-magnetite Janus nanostructures become lumino-magnetic which integrates the two most significant properties of a particle i.e. magnetic and optical into a single nanosystem. The quicker and higher response rate of the nanoparticles to alternating magnetic field opens up the possibility of these materials to be used for hyperthermia treatments. The further in vivo studies can be carried out in order to check the suitability of these nanomaterials as MRI contrast enhancement agents. It shows that silver integration imparts multimodality to the magnetite nanoparticle and makes them more feasible to be used for biomedical applications.

4. Conclusion

Magnetite nanoparticles integrated with silver nanoparticles were synthesized using a single-phase emulsion method and characterized for their various physical properties such as zeta potential, surface plasmon resonance peak and hyperthermic performance. The size of the Janus nanoparticles was observed to be of nanometer order which is an important criterion for cellular uptake. The silver integration also increased the colloidal stability of the Fe_3O_4 nanoparticles. The obtained nanostructures were found to show SPR band and luminescence peak in the visible range of the electromagnetic spectrum. The absolute increase in temperature and specific absorption rate were measured for the bare magnetite and silver-magnetite nanoparticle. The value of SAR is obtained to be 7.58 and 1.28 W g^{-1} for magnetite and silver-magnetite Janus nanoparticles, respectively. The experimental analyses of silver-magnetite nanoparticles suggest the feasibility of these nanoparticles as multimodal agents.

Acknowledgments

The authors are thankful to Central Instrument Facility Centre, Indian Institute of Technology, Banaras Hindu University, for providing TEM facilities.

ORCID iDs

Pinki Singh  <https://orcid.org/0000-0003-2837-9764>

Chandan Upadhyay  <https://orcid.org/0000-0002-8392-7236>

- G. F. Goya, T. S. Berquó, F. C. Fonseca, and M. P. Morales, "Static and dynamic magnetic properties of spherical magnetite nanoparticles," *J. Appl. Phys.* **94**, 3520 (2003).
- A. S. Teja and P. Koh, "Synthesis, properties, and applications of magnetic iron oxide nanoparticles," *Prog. Cryst. Growth Charact. Mater.* **55**, 22 (2009).
- J. Gao, H. Gu, and B. Xu, "Multifunctional magnetic nanoparticles: design, synthesis, and biomedical applications," *Acc. Chem. Res.* **42**, 1097 (2009).
- T. K. Jain, M. K. Reddy, M. A. Morales, D. L. Leslie-pelecky, and V. Labhasetwar, "Articles biodistribution, clearance, and biocompatibility of iron oxide magnetic nanoparticles in rats," *Mol. Pharm.* **5**, 316 (2008).
- M. Yamaura, R. L. Camilo, L. C. Sampaio, M. A. Macedo, M. Nakamura, and H. E. Toma, "Preparation and characterization of (3-aminopropyl) triethoxysilane-coated magnetite nanoparticles," *J. Magn. Magn. Mater.* **279**, 210 (2004).
- D. Bobo, K. J. Robinson, J. Islam, K. J. Thurecht, S. R. Corrie, and S. R. Corrie, "Nanoparticle-based medicines: a review of FDA-approved materials and clinical trials to date," *Pharm. Res.* **33**, 2373 (2016).
- D. K. Kim, Y. Zhang, W. Voit, K. V. Rao, and M. Muhammed, "Synthesis and characterization of surfactant-coated superparamagnetic monodispersed iron oxide nanoparticles," *J. Magn. Magn. Mater.* **225**, 30 (2001).
- A. Cervadoro, C. Giverso, and R. Pande, "Design maps for the hyperthermic treatment of tumors with superparamagnetic nanoparticles," *PLoS One* **8**, e57332 (2013).
- J. Reguera, D. Jiménez de Aberasturi, M. Henriksen-Lacey, J. Langer, A. Espinosa, B. Szczupak, C. Wilhelm, and L. M. Liz-Marzán, "Janus plasmonic-magnetic gold-iron oxide nanoparticles as contrast agents for multimodal imaging," *Nanoscale* **9**, 9467 (2017).
- S. Lee, R. G. Thomas, M. J. Moon, H. J. Park, I. Park, B. Lee, and Y. Y. Jeong, "Near-infrared heptamethine cyanine based iron oxide nanoparticles for tumor targeted multimodal imaging and photothermal therapy," *Sci. Rep.* **7**, 2108 (2017).
- A. Gnach and A. Bednarkiewicz, "Lanthanide-doped up-converting nanoparticles: merits and challenges," *Nano Today* **7**, 532 (2012).
- P. Singh and C. Upadhyay, "Size selectivity of magnetite core- (Ag/Au) shell nanoparticles for multimodal imaging applications," *Mater. Res. Express* **4**, 105401 (2017).
- P. Singh, B. K. Gupta, N. K. Prasad, P. K. Yadav, and C. Upadhyay, "Novel facets of multifunctional Ag @ Fe_3O_4 core-shell nanoparticles for multimodal imaging applications," *J. Appl. Phys.* **124**, 074901 (2018).
- P. Singh and C. Upadhyay, "Role of silver nanoshells on structural and magnetic behavior of Fe_3O_4 nanoparticles," *J. Magn. Magn. Mater.* **458**, 39 (2018).
- W. F. C. Sager, "Microemulsion templating," *Schr. Forschungszent. Juelich, Mater. Mater.* **10**, A6/1 (2002).
- A. L. Patterson, "The scherrer formula for X-ray particle size determination," *Phys. Rev.* **56**, 978 (1939).
- S. Pabisch, B. Feichtenschlager, G. Kickelbick, and H. Peterlik, "Effect of interparticle interactions on size determination of zirconia and silica based systems—a comparison of SAXS, DLS, BET, XRD and TEM," *Chem. Phys. Lett.* **521**, 91 (2012).
- D. Hanaor, M. Michelazzi, C. Leonelli, and C. C. Sorrell, "The effects of carboxylic acids on the aqueous dispersion and electrophoretic deposition of ZrO_2 ," *J. Eur. Ceram. Soc.* **32**, 235 (2012).
- R. W. O. Brien, B. R. Midmore, A. Lamb, and R. J. Hunter, "Electroacoustic studies of moderately concentrated colloidal suspensions," *Faraday Discuss. Chem. Soc.* **90**, 301 (1990).
- N. A. Monteiro-Riviere and C. L. Tran, *Nanotoxicology: Characterization* (Informa Healthcare USA, Inc., New York, 2007).
- Y. Zhang, M. Yang, and N. G. Portney, "Zeta potential: a surface electrical characteristic to probe the interaction of nanoparticles with normal and cancer human breast epithelial cells," *Biomed. Microdevices* **10**, 321 (2008).
- P. K. Jain, K. S. Lee, I. H. El-sayed, and M. A. El-sayed, "Calculated absorption and scattering properties of gold nanoparticles of different size, shape, and composition: applications in biological imaging and biomedicine," *J. Phys. Chem. B* **110**, 7238 (2006).
- A. J. Haes and R. P. V. Duyne, "A nanoscale optical biosensor: sensitivity and selectivity of an approach based on the localized surface plasmon

- resonance spectroscopy of triangular silver nanoparticles,” *J. Am. Chem. Soc.* **124**, 10596 (2002).
- 24) J. Tauc, R. Grigorovici, and A. Vancu, “Optical properties and electronic structure of amorphous germanium,” *Phys. Status Solidi* **15**, 627 (1966).
- 25) J. Zaanen, G. A. Sawatzky, and J. W. Allen, “Band gaps and electronic structure of transition-metal compounds,” *Phys. Rev. Lett.* **55**, 418 (1985).
- 26) L. Wang and H. S. Zhou, “Green synthesis of luminescent nitrogen-doped carbon dots from milk and its imaging application,” *Anal. Chem.* **86**, 8902 (2014).
- 27) S. K. Bhunia, N. Pradhan, and N. R. Jana, “Vitamin B1 derived blue and green fluorescent carbon nanoparticles for cell-imaging application,” *ACS Appl. Mater. Interfaces* **6**, 7672 (2014).
- 28) A. Muela, D. Mun, R. Mart, I. Orue, E. Garaio, A. Abad, J. Alonso, A. Jose, and M. L. Fdez-gubieda, “Optimal parameters for hyperthermia treatment using biomineralized magnetite nanoparticles: theoretical and experimental approach,” *J. Phys. Chem. C* **120**, 24437 (2016).
- 29) S. Huang, S. Y. Wang, A. Gupta, D. A. Borca-Tasciuc, and S. J. Salon, “On the measurement technique for specific absorption rate of nanoparticles in an alternating electromagnetic field,” *Meas. Sci. Technol.* **23**, 1 (2012).